Excess Electron in Water at Different Thermodynamic Conditions†

Mauro Boero‡

Center for Computational Sciences, University of Tsukuba, Tennodai 1-1-1, Tsukuba, Ibaraki 305-8577, Japan, Graduate School of Pure and Applied Sciences, University of Tsukuba, 1-1-1 Tennodai, Tsukuba, 305-8571, Japan, and CREST, Japan Science and Technology Agency, 4-1-8 Honcho, Kawaguchi, Saitama 332-0012, Japan

Received: June 5, 2007; In Final Form: July 26, 2007

A hydrated electron in water at different densities and temperatures is studied via a set of density functional based molecular dynamics simulations, showing that a localization of an excess electron is still present even at very low densities. Space variations of the molecular dipole moments are analyzed, proposing a simple algorithm to identify the region of localization of the wavefunction relative to the solvated electron in terms of orientation of the H_2O molecular dipole moments. Finally, the effects of the self-interaction corrections on the optical absorption spectra are analyzed and compared with both available experimental data and path integral molecular dynamics calculations, showing that a weighted subtraction of the self-interaction yields a systematic improvement in the position of the absorption peak.

1. Introduction

It has now been more than 40 years[1] in which excess electrons in aqueous solution have been intensely investigated experimentally[1−8] and theoretically.[9−17] Nonetheless, despite such a long history, excess electrons still represent a particularly active research field, because they are ubiquitous in liquid phases, in electron-transfer processes in solution, in photobiochemistry, and in a wide variety of aqueous reactions.[18−25] A wealth of accurate experiments have been conducted over the years, focusing on photoionization of normal and heavy water at ordinary liquid conditions[1−4] ($T = 300$ K, $\rho = 1.0$ g/cm^3) and charged $(H_2O)_n^-$ clusters.[7,8] More recently, complex solution chemistry reactions involving hydrated electrons are being pioneered, the most relevant examples being pulse radiolysis of polar molecules[18] and transition state spectroscopy of photoexcitation of negative ions in solution.[19] Looking at the rich literature reveals the general picture that an excess electron in water, $(e^-)_{aq}$, is stabilized in a cavity that can be either preexistent or cleaved *ad hoc* to accommodate this additional charge over a femtosecond time scale.[9−11] These short stabilization times are of the same order of magnitude of the molecular rotation times[26] and thus dependent on the thermodynamic state of the fluid. The accommodation of the extra electron in the solvent interrupts locally the hydrogen bond (H-bond) network either of the extended liquid or of the water cluster[12−15] and the surrounding H_2O molecules reorient and polarize around a sort of bubble, representing the excess electron charge distribution. This $(e^-)_{aq}$ forms a typical anionic solvation shell, in which the slightly positive H atoms of the solvating H_2O molecules, or at least one of the two of them, points toward the cavity. The number of H_2O monomers composing the first solvation shell has been shown to depend on the size of the water cluster[13] or on the density of the fluid.[15] These atomic scale models, resulting from dynamical simulations, are generally probed by the calculation of the related optical absorption spectra, a quantity that represents the direct outcome of experiments.[2−8]

More recently, the emerging field of supercritical water promoted synthetic reactions[27−31] has given a renovated impulse to these studies toward a new direction, in a region of the phase space diagram of water with uncommon, and often unexpected, properties. Pioneering experimental studies of the absorption spectra due to excess electrons in nearly supercritical water were reported by Gaathon, Czapski, and Jortner;[25] in these studies, it was evidenced for the first time that the peak of the absorption curve shifts toward lower energy, $\hbar\omega$, values by decreasing the density of the solvent; on the basis of those measurements, it was argued that a certain degree of localization of $(e^-)_{aq}$ persists also at very low densities, which are typical of the supercritical state in the proximity of the critical point. This inferred microscopic picture had to wait about 30 years before being studied at an atomistic level by path integral molecular dynamics making use of a SPC classical force field[27] and by first principles molecular dynamics simulations.[15] Yet, several open issues and inherent technical difficulties make these investigations among the most demanding tasks in the field of computer simulations.

The scope of the present simulations is to provide a systematic analysis of the $(e^-)_{aq}$ solvation properties at different thermodynamic conditions via first-principles molecular dynamics, focusing on two issues. The first one is the identification of the localization region of the electron density, not always evident from a simple inspection of the related Kohn−Sham (KS) orbitals. To this aim, a simple algorithm making use only of the molecular dipole moments, available at each simulation step, and the definition of a direct and reciprocal space mesh, is presented and discussed, offering a tool to select appropriate configurations from the trajectories. The second issue is the effect of the self-interaction corrections on the computed absorption spectra. In fact, present-day DFT functionals have a well-known drawback in describing unpaired electrons, with a pronounced pathology for radicals, because of the incomplete cancellation of the electron self-interaction that tends to delocalize charge.[32] To overcome this difficulty, a slight modification of a self-interaction correction scheme recently introduced[33] is

† Part of the "Giacinto Scoles Festschrift".

‡ E-mail: boero@comas.frsc.tsukuba.ac.jp.

10.1021/jp074356+ CCC: $37.00
Published on Web 09/21/2007

adopted, to check its effect on the electronic density of states and the related optical absorption spectrum.

2. Computational Details

Simulations were performed within the Car−Parrinello molecular dynamics (CPMD) framework[34,35] on 32-molecule H_2O systems at different densities and temperatures.[36−38] Before the addition of the excess electron, the water systems were equilibrated for 9 ps.[39,40] Subsequently, one extra electron was introduced, the system was re-equilibrated, and statistics were collected for about 10 ps. Because the addition of one electron implies a total net charge $Q = -1$, a compensating uniform background charge ensured the formal neutrality of the system and avoided spurious interactions with neighbor images, because periodic boundary conditions are applied. Three thermodynamic states have been considered: A normal liquid at $T = 300$ K, $\rho = 1.00$ g/cm^3 in a cubic simulation cell of side $L = 9.865$ Å, hereafter labeled as NLW, a high-density supercritical water (HDSW) system at $T = 653$ K and $\rho = 0.73$ g/cm^3, as typically used in synthetic reaction experiments, in a cubic box of lateral size $L = 10.943$ Å, and a low-density supercritical water (LDSW) system at $T = 653$ K, $\rho = 0.32$ g/cm^3, $L = 14.375$ Å, close to the experimental critical point. The temperature was controlled by a Nosé−Hoover chain thermostat on the ionic degrees of freedom.[41−43]

The Kohn−Sham wavefunctions representing all the valence electrons plus the additional e^-, were expanded in a plane wave basis set with an energy cutoff of 70 Ry and the Brillouin zone was sampled at the Γ point only. In all the density functional (DFT) calculations performed, the many body effects are approximated in the standard way, by including gradient corrections after Becke[44] and Lee−Yang−Parr[45] on the exchange and correlation functionals, respectively; because one singly occupied level exists due to the excess electron, an unrestricted spin approach was adopted. The 1s core electrons of oxygen are not included and the core-valence interaction is described by a norm-conserving Troullier−Martins[46] pseudopotential for O, whereas an analytical Car−von Barth[47] potential is adopted for hydrogen, to eliminate the divergence at $r = 0$ of the bare Coulomb potential. The CPMD equations of motion for both electrons and ions are integrated numerically by finite differences via a velocity Verlet algorithm. The integration time step used in this discretization was set to $\Delta t = 3.0$ au (0.072 fs) and the fictitious electronic mass was chosen to be $\mu = 380$ au; these parameters have been shown to ensure good control of the conserved quantities.[48] Analyses of the molecular dipole moments and electronic structure evolution were done via maximally localized Wannier functions (WF) and related Wannier function centers (WFC),[49] which involve just a unitary transformation of the Kohn−Sham eigenstates of the Hamiltonian. These provide an unbiased way to partition the total charge density and to compute directly the center of mass and the related spread[50] of the electron square modulus wavefunctions whenever the corresponding eigenstates of the Kohn−Sham Hamiltonian are well localized.[37]

The self-interaction corrections (SIC) were accounted for according to the functional scheme

$$E^{\mathrm{SIC}}[\rho_{\mathrm{spin}}] = -a_{\mathrm{SIC}}E^{\mathrm{H}}[\rho_{\mathrm{spin}}] - b_{\mathrm{SIC}}E^{\mathrm{xc}}[\rho_{\mathrm{spin}}] \qquad (1)$$

where $\rho_{\mathrm{spin}} = \rho_\alpha - \rho_\beta$ is the electron spin density, E^{H} is the Hartree functional, and E^{xc} is the exchange and correlation functional. Different values of the adjustable pre-factor a_{SIC} were tested, assuming $b_{\mathrm{SIC}} = 0$, which does not represent a significant limitation, as explained in ref 33. Further computational details will be given in the next paragraphs as a support to the discussion.

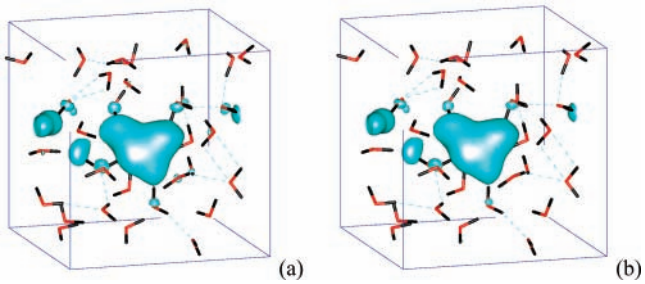

Figure 1. Kohn−Sham (KS) state of a localized hydrated electron corresponding to the highest occupied orbital in HDSW (a) and total spin density (b). H_2O molecules are shown as v-shaped sticks, and the electronic densities, in blue, are plotted at an isosurface value of 1×10^{-5} e/Å^3. The atoms color code is red for O and black for H, and dashed lines show the hydrogen bonds

3. Results and Discussion

3.1. Characterization of the Solvated Electron and Hydrogen Bond Network Topology. As noted elewhere,[15] the addition of an excess electron to a NLW systems requires about 1.6 ps to allow the H-bond network to rearrange and accommodate $(e^-)_{\mathrm{aq}}$ in a cavity where, on average, six H_2O water molecules form an ionic solvation shell pointing at least one of the H atoms toward the region where the excess electron is localized. However, by monitoring the trajectory and the related electronic states, it was noticed that such a localization lasts for a short time τ_{loc}, namely, 50 fs $< \tau_{\mathrm{loc}} <$ 90 fs. After this time the localized single lobe of the $(e^-)_{\mathrm{aq}}$ electron distribution becomes dispersed and re-forms in another region of the system where a new cavity is cleaved. A similar picture holds also in HDSW, where, however, the lower density is responsible for the presence of pre-existing cavities[15,40] where the additional electron can be accommodated more easily. At the same time, density fluctuations and a temperature higher with respect to NLW make the localization time shorter ($\tau_{\mathrm{loc}} < 30$ fs). The localization of $(e^-)_{\mathrm{aq}}$ becomes even more problematic when the density lowers to 0.32 g/cm^3 (LDSW), where the H-bond network is disrupted and the density so low that in practice only small clusters can be formed, namely dimers, trimers, and more rarely tetramers.[39,40] In these conditions, large vacuum regions are present and the excess electron can be easily accommodated in the system. Nevertheless, it is still possible to identify single lobes despite the fact that the solvation shell is generally larger and composed of a few molecules in a sense that will be better quantified in the next paragraphs. These broad single lobe distributions survive for less than 15 fs, before being re-formed elsewhere as a consequence of the rapid density fluctuations and highly disrupted H-bond network.

In the present work, as well as in ref 15, the maximally localized WFs[49] are used to characterize the solvated electron whenever the corresponding Kohn−Sham orbital, representing the variational basis set in the Car−Parrinello molecular dynamics, shows a good localization,[50] as in the snapshot shown in panel a of Figure 1.

The square modulus of the highest occupied orbital, $|\psi^{\mathrm{KS}}{}_{\mathrm{sol}}(\mathbf{r})|^2$, coincides in practice with the total spin density of the system shown in panel b of the same figure, where the only noticeable difference is the disappearance of some σ^*-like contributions on a few H_2O molecules around the main lobe in $\rho_{\mathrm{spin}}(\mathbf{r}) = \rho_\alpha(\mathbf{r}) - \rho_\beta(\mathbf{r})$ with respect to $|\psi^{\mathrm{KS}}{}_{\mathrm{sol}}(\mathbf{r})|^2$. In the case

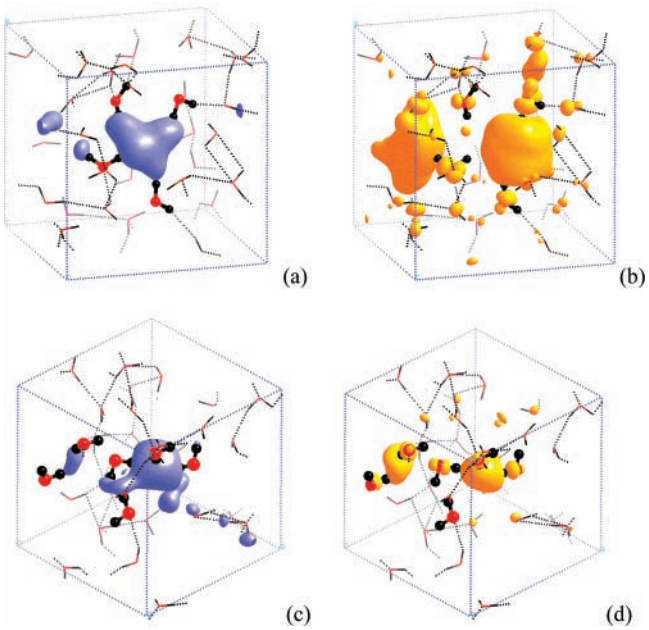

Figure 2. (a) and (b) show the Wannier function of a localized hydrated electron and the lowest unoccupied orbital, respectively, for the same HDSW configuration shown in the previous figure. When the electron becomes delocalized and the solvation shell breaks apart, the Wannier functions of the solvated electron (c) and of the lowest unoccupied orbital (d) lose their s-like and p-like character, respectively, and become meaningless. Blue isosurfaces refer to the occupied solvated electron state, and yellow ones, to the lowest unoccupied state; both are shown at 1×10^{-5} e/Å^3. Thick sticks and ball show the H_2O molecules belonging to the first solvation shell of the hydrated electron, and the rest of the solvent is shown as thin sticks. The atoms color code is the same used in Figure 1.

of localized orbitals, an unbiased partitioning of the total charge is achieved by the use of WFs and related WFCs, that give a geometrical identification of the solvated electron and provide molecular dipole moments of all the H_2O monomers of the system *on the fly* during the simulation,[37] in terms of WFCs positions and ionic coordinates, as described in detail in ref 49. Furthermore, WFCs of $(e^-)_{aq}$ allow for the construction of pair correlation functions and characterization of the solvation shell, as will be shown in the ongoing discussion. When an electron is well localized (Figure 1), the corresponding WF (Figure 2a) gives a main lobe in the accommodating cavity similar to $|\psi^{KS}_{sol}(\mathbf{r})|^2$ and the characterization of the solvation shell via WFCs becomes possible. In these conditions, the general scenario depicted by the group of Rossky[9−11] holds also in supercritical water. Namely, the wavefunction of $(e^-)_{aq}$ acquires a sort of s-like character with a more or less isotropic distribution inside the cavity and the three associated lowest unoccupied orbitals resemble a sort of p-like states with a node in the cavity and two main lobes, and also with several σ^* contributions on other water molecules around (Figure 2b). These characteristics may be rapidly lost, especially in HDSW and LDSW, and for a certain number of configurations, the Kohn−Sham half occupied $(e^-)_{aq}$ state becomes rather dispersed. As a consequence, the corresponding Wannier states become meaningless, having an undefined character as shown in panels c and d of Figure 2. In these conditions, the WFCs cannot be used to characterize solvation shells or to construct radial distribution functions. This qualitative statement can be made more quantitative by analyzing the spread[50] associated with the WFs of the excess electron. In all the cases analyzed in which a good localization was found, this spread amounts to 1.34 ± 0.08 Å in NLW, 1.36 ± 0.10 Å in HDSW, and 1.42 ± 0.14 Å in LDSW. Conversely, in the cases of delocalization of the $(e^-)_{aq}$ state, these spreads range from 4.44 Å to more than 6 Å, i.e., on a substantial part of the volume of the simulation cell, showing that WFs and WFCs become useless and the related configurations must be discarded in the analysis of the solvation properties.

The search for the configurations in which $(e^-)_{aq}$ is well localized was indeed one of the most demanding tasks in the present analysis. On one hand, one has to extract uncorrelated configurations and fully diagonalize the KS Hamiltonian, avoided in Car−Parrinello molecular dynamics. On the other hand, WFCs are available at each step of the simulation, and they are certainly correct as far as the σ-states and lone pairs of water molecules are concerned,[37] but insufficient and sometimes even misleading for $(e^-)_{aq}$ in the sense discussed above. In practice, one of the problems to face is a clear identification from the trajectories of those cavities in which a localized $(e^-)_{aq}$ can be accommodated and that are accompanied by some local modifications of the H-bond network topology. An analysis of the magnitude of the molecular dipole moments $\mathbf{p}_w$ of the single H_2O monomers has shown that water molecules of the first solvation shell of $(e^-)_{aq}$ do not display any significant variation in terms of the absolute value of $\mathbf{p}_w$ with respect to the rest of the solvent, and these values fit perfectly in the distributions typical of the thermodynamic state considered.[39,40] This is not entirely unexpected, because several experiments have already shown rather clearly that the value of the molecular dipole moment of H_2O molecules is mainly due to the extension of the H-bond network.[51,52] Thus, $|\mathbf{p}_w|$ seems unable to discriminate between the presence or absence of $(e^-)_{aq}$. Naively, it can be noticed that the presence of a negative charge represented by $(e^-)_{aq}$ has at least the effect of changing the local topology of the H-bond network and the orientation of two contiguous molecular dipole moments, as shown schematically in Figure 3.

It seems then that it is the local (relative) orientation of $\mathbf{p}_w$ that can offer a clue to identify a localized hydrated electron, rather than its magnitude. By visualizing the molecular dipole as a vector attached to each molecule, one could in principle sort out the region where $(e^-)_{aq}$ is localized. However, for large systems containing many water molecules and/or long trajectories with a high number of configurations rapidly changing, as in the low-density/high-temperature supercritical states, this turned out to be not very practical and not free from ambiguities. In an attempt to simplify this task and make use of these space variations of the dipole moment, one can multiply $\mathbf{p}_w$ by a trigonometric function or, better, in a complex domain, by a phase factor $e^{i\mathbf{G}(\mathbf{r}-\mathbf{R}w)}$ that keeps into account the space variations of $\mathbf{p}_w$ around the center of mass of the water molecule. Because a reciprocal space mesh is generally constructed in these kind of simulations, the dependence on a specific $\mathbf{G}$ vector can be eliminated by a summation on $\mathbf{G}$, leading to a dipole moment distribution function as a weighted superposition of $\mathbf{p}_w$,

$$\mathbf{P}(\mathbf{r}) = \sum_{\mathbf{G}} \sum_{w=1}^{N^{wat}} \mathbf{p}_w \exp[i\mathbf{G}\cdot(\mathbf{r} - \mathbf{R}_w)] \qquad (2)$$

where the index w runs over all the N^{wat} water molecules. In the numerical implementation, beause the center of mass of an H_2O molecule, $\mathbf{R}_w$, coincides in practice with the position of the oxygen, N^{wat} is just the number of O atoms present in the system and $\mathbf{R}_w$ is their Cartesian positions. The function defined in this way can be easily constructed from the Wannier function centers (WFCs) and the atomic positions,[48] computed and printed at each simulation step. The problem is that if a very

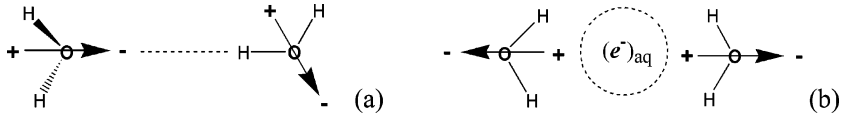

Figure 3. Schematic representation of the orientation of the molecular dipole moments along a regular linear H-bond (a) and in the presence of a solvated electron accommodated between two H_2O molecules (b). The arrows indicate the direction of the molecular dipole moment with the charge sign at both the end points.

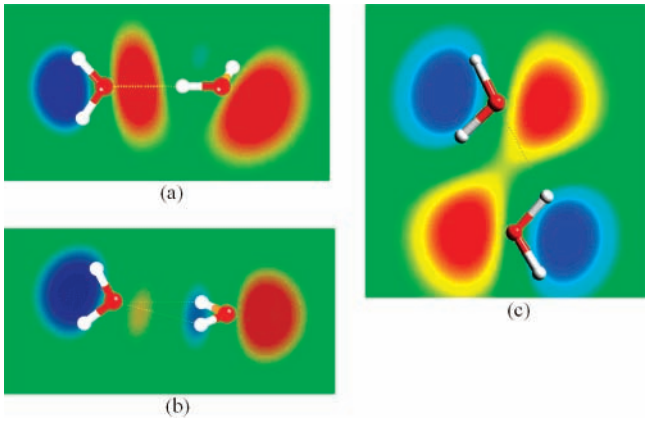

Figure 4. Divergence of the dipole moment distribution function for a linear H-bond (a), a bifurcated H-bond (b), and a cyclic H-bond (c). The contour color maps range from positive (blue) to negative (red) values, the green color representing the zero. Water molecules are shown as stick and balls, where the red balls refer to O and the white ones to H.

fine mesh is used or, analytically speaking, if the limit $\mathbf{G} \rightarrow \infty$ is computed, the summation on the **G**-vectors reduces to a Dirac delta

$$\delta(\mathbf{r} - \mathbf{R}_w) = \frac{1}{\pi^3} \sum_{\mathbf{G}=0}^{\infty} e^{i\mathbf{G}(\mathbf{r}-\mathbf{R}_w)} \tag{3}$$

To overcome the problem of a not very useful point-like distribution, it is possible to add a Gaussian spread as

$$\mathbf{P}(\mathbf{r}) = \sum_{\mathbf{G}} \sum_{w=1}^{N^{wat}} \mathbf{p}_w \exp[i\mathbf{G}(\mathbf{r} - \mathbf{R}_w)] \cdot e^{-\lambda^2 G^2} \tag{4}$$

that does not add a significant computational cost, because the Gaussian weight depends only on the square norm of the vectors **G**. The parameter λ is of the order of the O−H bond length (∼1 Å) and allows for a better space separation of the dipole contribution of each molecule with respect to the global superposition. In the present case, for convenience and consistency, the vectors **G** are the reciprocal space vectors used in the plane wave expansion, explicitly defined by the components $G_j = (2\pi/L)n_j$ ($j = x, y, z$; $n_j = 0, ..., N_{cutoff}$). However, none of these quantities is actually dependent on the simulation framework adopted and any approach in which molecular dipole moments are provided and a sufficiently dense reciprocal space mesh can be defined allows for the construction of **P**(**r**) according to eq 4; this is, for instance, the case of classical polarizable force fields.

Because space variations in the orientation of the dipole, i.e., mathematically speaking, $\partial/\partial\mathbf{r}$, is what one wants to focus on, a better suited quantity is the divergence of **P**(**r**),

$$\nabla \cdot \mathbf{P}(\mathbf{r}) = \sum_{\mathbf{G}} e^{i\mathbf{G}\cdot\mathbf{r}} (i\mathbf{G} \cdot \sum_{w=1}^{N^{wat}} \mathbf{p}_w \exp[i\mathbf{G} \cdot \mathbf{R}_w] \cdot e^{-\lambda^2 G^2}) \tag{5}$$

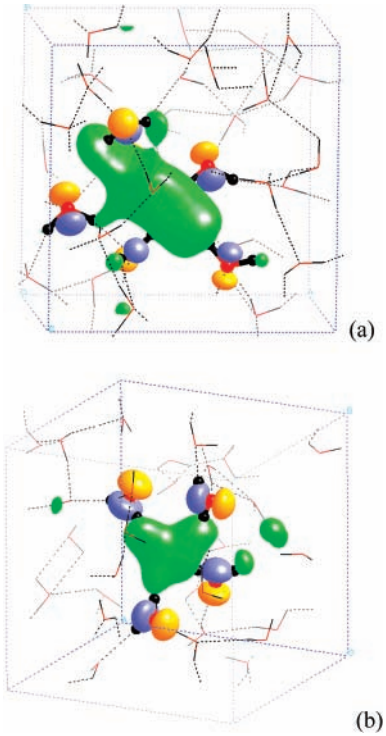

Figure 5. Divergence of the div[**P**(**r**)] dipole moment function for an electron solvated in NLW (a) and in HDSW (b). The Wannier functions of the related electron distributions are plotted as green isosurfaces at 1×10^{-5} e/Å^3, the blue (positive) and yellow (negative) bubbles on top of the water molecules of the first solvation shell represent the isosurfaces of div[**P**(**r**)] at ±0.1 D/Å. Water molecules belonging to the first solvation shell of the hydrated electron are shown as thick sticks and balls, and the rest of the solvent is in thin sticks. The color code is red for O and black for H, and dashed lines indicate hydrogen bonds.

and which is simply a Fourier transform of a scalar product. Applied to typical H-bond configurations in supercritical water,[39] the result of eq 5 can be visualized in terms of density maps, as shown in Figure 4. This makes easier the identification of the solvating cavities and circumvent the problem of inspecting one-by-one the single molecular dipole moments and their relative orientations.

This simple algorithm is able to capture the local H-bond topology, and the single scalar field represented by the divergence of **P**(**r**) provides all the details of the local $\mathbf{p}_w$ orientation in terms of a single density map. In fact, in any H-bond configuration, one can see an alternating sequence of positive (blue) and negative (red) regions. When an excess electron localizes in a cavity, instead, water molecules are generally polarized with the positive terminal H atoms pointing toward the space among the H_2O molecules where $(e^-)_{aq}$ is accommodated. This represents a typical anionic solvation shell, and in a sense, it is an anomaly in the alternating positive/negative sequence, thus allowing for the identification of the localized $(e^-)_{aq}$. Two examples are reported in Figure 5 for NLW and HDSW, along with the corresponding Wannier functions of $(e^-)_{aq}$.

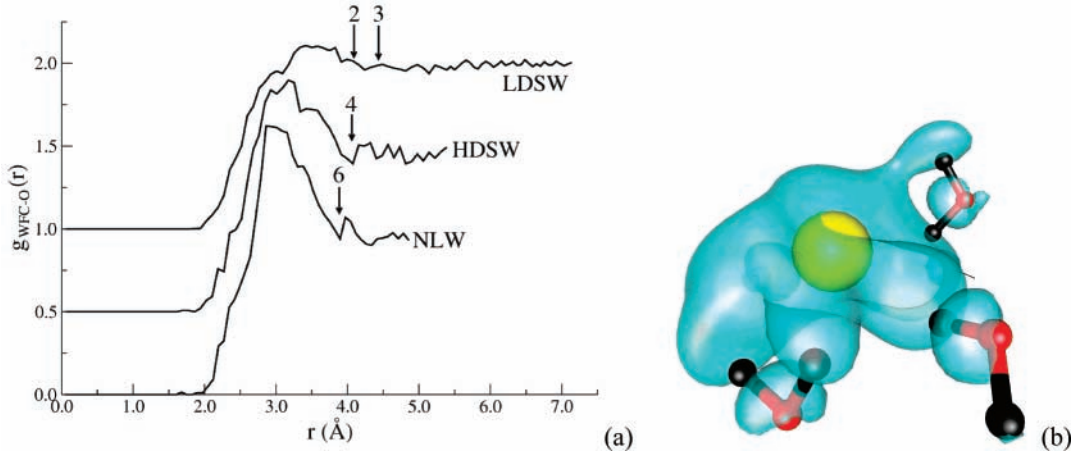

Figure 6. (a) Pair correlation functions $g_{WFC-O}(r)$ between the Wannier function center (WFC) of the hydrated electron and the O atoms of the surrounding H_2O molecules for the three thermodynamic states of water. The numbers above the arrows indicate the coordination number and pair correlation functions of HDSW and LDSW have been shifted along the *y*-axis for clarity. The snapshot in (b) shows the hydrated electron in LDSW in the case of full localization The isosurface (blue cloud) is shown at 1×10^{-5} e/Å^3, and the yellow ball at the center represents the Wannier function center. Three H_2O molecules form the solvation shell in this case.

By decreasing the isosurface value or the localization parameter λ, it is indeed possible to visualize a basin in which the negative amplitudes of the divergence of $\mathbf{P}(\mathbf{r})$, that appear localized only in the neighborhood of the H_2O molecules in Figures 5, overlap into a region as large as the cavity. This simple mathematical tool makes possible a screening of the configurations printed in the trajectory *on the fly*, without computing and storing wavefunctions at each step, or can be used as complementary information to inspect the H-bond network topology of a general polar solvent. For instance, because molecular dipole moments are available at each step of the dynamics, this algorithm, although more qualitative than quantitative, represents a convenient tool to discriminate on which configurations a full diagonalization of the KS Hamiltonian and related calculation of the unoccupied states are meaningful and worthy of computational effort.

The amount of localization of $(e^-)_{aq}$ at the various thermodynamic states can also be quantified in terms of ground state radius according to the definition given in ref 10,

$$\langle r \rangle = \langle \int_\Omega |\psi_{sol}^{KS}(\mathbf{r})|^2 \mathbf{r}^2 \, d^3r \rangle^{1/2} \qquad (6)$$

where Ω is the volume of the simulation cell and ψ_s is the wavefunction of $(e^-)_{aq}$. Averaging over 50 uncorrelated configurations extracted from the trajectories obtained from the present set of simulations, the ground state radius and relative standard deviation turned out to be $\langle r \rangle = 2.2 \pm 0.2$ Å in the case of NLW, in rather good agreement with the value of 2.1 obtained from path integral simulations.[10] The solvated electron shows a broader distribution in HDSW, $\langle r \rangle = 2.6 \pm 0.4$ Å, which enhances further in LDSW, $\langle r \rangle = 3.3 \pm 0.5$ Å. The overall picture offered by these estimations is a broadening of the electron distribution of $(e^-)_{aq}$ upon reduction of the density of the solvent. This is confirmed by an analysis of the solvation shell of $(e^-)_{aq}$ in terms of pair correlation functions (PCFs), assuming as a reference point the WFC associated to the hydrated electron and computing its distances from the O atoms of the surrounding water molecules. The presence of only one WFC per configuration leads to limited statistics; however, the main features are captured, as evidenced also in another analogous problem dealing with protons in solution.[53] The resulting PCF is shown in panel a of Figure 6. It can be seen that the PCF becomes less structured by decreasing the density and the first WFC−O peak decreases in maximum value as well as broadens, displaying a slight shift toward larger values. However even at the lowest density, it does not disappear completely, suggesting that a solvation shell still can be formed even at very low densities.

By integrating the PCFs, the qualitative picture given in the snapshots of Figure 5 can be made more quantitative: in the case of NLW, the first solvation shell of $(e^-)_{aq}$, provided that it is well localized in a cavity, is composed of six H_2O molecules, whereas, in HDSW, four water molecules compose the solvation shell of $(e^-)_{aq}$. At 0.32 g/cm^3 (LDSW) the solvation shell is reduced to only three, or sometimes two, water molecules, yet a certain localization of $(e^-)_{aq}$ is still present, and this provides a microscopic support to the conclusion inferred from transient IR absorption measurements in near critical low-density water.[25] It must be acknowledged that the case of LDSW was indeed the most difficult to analyze; on one hand, the low density implies that extended vacuum regions are present and the H-bond network is reduced to small clusters;[39,40,51] thus only a few H_2O molecules can concur to form a solvation cage inside which $(e^-)_{aq}$ is localized. On the other hand, the short localization time ($\tau_{loc} < 15$ fs) and the fast density fluctuations allow the electronic wavefunction ψ_{sol}^{KS} to spread and delocalize easily, spending longer times in a delocalized state. The disruption of the salvation shell makes it difficult to clearly identify a first minimum and, upon integration, a well-defined plateau where the integrated coordination number assumes an unambiguous integer value. Hence, the arrows above the LDSW curve in Figure 6 must be intended just as a range in which the coordination number makes an almost continuous transition from 2 to 3. As mentioned, in all the configurations analyzed, the first solvation shell of the hydrated electron turns out to be rather disrupted and broader than at higher density, a fact that can be intuitively expected. In the cases in which a defined localization was found, the wavefunction of $(e^-)_{aq}$ is surrounded by two or three solvating H_2O molecules, as sketched in panel b of Figure 6 and generally more than one H of the solvating H_2O molecules points toward the electronic cloud representing the hydrated electron. This snapshot is rather representative of the general solvated electron structure in LDSW, and it is easy to recognize that it is indeed a collective state generated by the overlap of the well-known lowest unoccupied molecular orbitals extending between the two terminal H atoms of an isolated H_2O molecule,

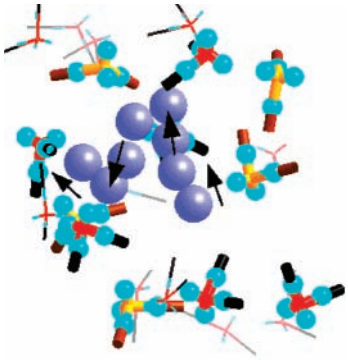

Figure 7. Displacement of the Wannier center of the hydrated electron (large blue ball) during the dynamics in HDSW. The arrows indicate the direction of the displacement. Red-black sticks show water molecules of the first solvation shell in the initial configuration, and yellow-brown sticks refer to the final configuration. Cyan spheres are the Wannier centers of the solvating H_2O molecules, and thin sticks are surrounding water molecules of the system not belonging to the first solvation shell.

as reported in any textbook. As a matter of curiosity, it can also be noted that whenever a localized $(e^-)_{aq}$ is present, the evolution of its corresponding Wannier center, $\mathbf{r}^{WFC}$, can be monitored as a function of time and its derivative $d\mathbf{r}^{WFC}/dt$ computed numerically and averaged as

$$\left\langle \left| \frac{d\mathbf{r}^{WFC}}{dt} \right| \right\rangle = \left\langle \frac{|\mathbf{r}^{WFC}(t+\Delta t) - \mathbf{r}^{WFC}(t)|}{\Delta t} \right\rangle \qquad (7)$$

Δt being the time increment between two successive configurations in which the same single lobe and first solvation shell propagate.

An example is shown in the superimposed snapshots of Figure 7, and the computed values of such a "random current" turned out to be 5.8 ± 2.0 and 10.4 ± 2.5 Å/ps in NLW and HDSW, respectively. A rough estimation of the corresponding current density, $\langle J^{WFC} \rangle = e\langle |d\mathbf{r}^{WFC}/dt| \rangle / L^3$, for the specific systems considered here, gives $9.6 \pm 3.0 \times 10^6$ (NLW) and $12.7 \pm 3.1 \times 10^6$ A/cm^2 (HDSW). Although not particularly instructive in this case, in the presence of an external electric field, one can follow the dynamical displacement of a localized charge and compute in an easy way the associated current density, a quantity that can be directly compared to experiments.

3.2. Optical Spectra and Self-Interaction Effects. As already reported in former works,[15,27] the major contributions to the optical spectrum come from the transitions from the singly occupied KS orbital of the hydrated electron level to the next three lowest unoccupied KS states, which assume a p-like character in the cases in which $(e^-)_{aq}$ is fully localized inside a cavity (Figure 1). These are indeed the transitions responsible for the peak of the optical curve, which is the quantity directly provided by experiments.[1−7]

From the distribution of the KS levels, ϵ_i, computed on 50 uncorrelated configurations extracted from the 10 ps long trajectories, the density of states (DOS) can be evaluated according to the standard formula

$$\mathrm{DOS}(E) = \left\langle \frac{1}{N_w} \sum_i \delta(E - \epsilon_i) \right\rangle \qquad (8)$$

N_w being the number of molecules composing the system. The result is reported graphically in Figure 8 for the three thermodynamic points studied here and the curves resemble closely the DOS observed in ref 40 (Figure 4) for HDSW and LDSW.

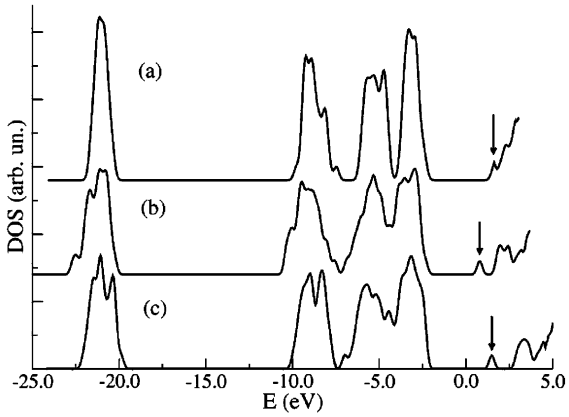

Figure 8. Density of states (DOS) for the three thermodynamic states of water discussed in the text: (a) LDSW; (b) HDSW; (c) NLW. The arrows indicate the peak of the solvated electron state corresponding to the highest occupied orbital.

In the case of NLW, the peak corresponding to the hydrated electron, indicated by an arrow in the figure, is located inside the gap at about 3.6 eV above the valence band of the lone pair orbitals, represented by the series of peaks between −10 and −2.5 eV along the energy axis. The lowest unoccupied states forming the peak at 3.4 eV are the p-like orbitals and represent the first pre-peak of the bulk conduction band. As mentioned above and discussed in a former work,[15] transitions from the $(e^-)_{aq}$ peak to these empty states represent the major contribution to the optical absorption spectrum. In fact, this is observed in femtosecond laser pulse spectroscopy experiments,[3,7] where the laser frequencies adopted fall in the range $\hbar\omega \sim 1.5-2.5$ eV $\ll E_{gap}$. A similar picture holds also in the case of HDSW, where the reduced density and the broadening induced by large dynamical fluctuations, shown in ref 40 (Figure 3), result in a slight shrinking of the energy gap. Yet, also in this case, the peak of the hydrated electron is located in the gap, at about 3.0 eV above the top of the valence band and 1.18 eV below the empty states peaks located in the range 1.9−2.4 eV on the energy axis of Figure 8. These peaks are again the p-like states although a broadening and a sort of splitting is visible in the DOS. This is mostly due to the anisotropy of the corresponding electron distribution in supercritical water system that has been discussed and quantified in detail in ref 15. When the density is close to the critical point, as in the LSDW system, the peak of $(e^-)_{aq}$ moves very close to the conduction band and seems to overlap the p-states peak, that, in turn, is reduced to a shoulder in curve (a) of Figure 8. This overlap, is, however, just a consequence of the statistical averaging. As shown in Figure 3 of ref 40, each single configuration presents a hydrated electron state separated by the conduction band bulk by about 0.5−0.7 eV but oscillates a lot because of the large density fluctuations. This $(e^-)_{aq}$ state is located very far from the valence band, by as much as 3.7 eV. As a word of warning, it must be noticed that the empty states band may depend on the size of the simulation cell, as remarked in ref 54, and energy shifts to different extents can affect the conduction band. This is not expected to alter qualitatively the picture discussed here in the case of the NLW state, because both the $(e^-)_{aq}$ and the empty p-states are well separated from each other and well resolved. For the HDSW and LDSW systems, due to the reduced density and consequent increased size of the simulation cell, these finite size effects are expected to be less important.

It is often claimed that self-interaction problems are present whenever an unpaired electron is treated within DFT approaches. In an attempt at inspecting whether or not this is the case, the

TABLE 1: Position of the Peak of the Absorption Spectrum of Water at Different Thermodynamic States and for Different Values of the Self-Interaction Correction Prefactor a_{SIC}

	NLW	HDSW	LDSW
no SIC	1.74	1.61	1.02
$a_{SIC} = 0.2$	1.73	1.58	1.01
$a_{SIC} = 0.3$	1.72	1.57	1.00
$a_{SIC} = 0.4$	1.71	1.57	1.00
$a_{SIC} = 0.5$	1.70	1.56	0.99
$a_{SIC} = 0.6$	1.70	1.56	0.99
$a_{SIC} = 0.7$	1.69	1.56	0.98
path integral MD	2.10[a]		0.95[a]
experiment	1.72[b]	1.0[c]	

[a] Reference 27. [b] Reference 3. [c] Reference 25, the closest system being $T = 618$ K and $\rho = 0.65$ g/cm^3.

effect due to the electronic self-interaction correction was studied in terms of optical transitions from the singly occupied level of $(e^-)_{aq}$ to its lowest lying empty states, because these provide a direct contact with experiments. The self-interaction scheme adopted here is a slight generalization of the formulation reported in ref 33 and written explicitly in eq 1. At variance with that case, in the present calculations the SIC was not applied only to the last half occupied state, as done in the original work of VandeVondele and Sprik. Instead, following the general idea of d'Avezac and co-workers, the SIC is applied to the full Kohn−Sham electronic potential $V^{KS}_{\alpha,\beta}(\mathbf{x})$ leading to a set of equations similar to those introduced in ref 55

$$V^{KS}_{\alpha}(\mathbf{x})\left|\psi^{\alpha}_i\right\rangle \rightarrow \left\{V^{KS}_{\alpha}(\mathbf{x}) - a_{SIC}\frac{\delta E^{H}[\rho_{spin}]}{\delta \rho_{spin}}\right\}\left|\psi^{\alpha}_i\right\rangle \qquad \forall\ \alpha \text{ spin}$$

$$V^{KS}_{\beta}(\mathbf{x})\left|\psi^{\beta}_i\right\rangle \rightarrow \left\{V^{KS}_{\alpha}(\mathbf{x}) + a_{SIC}\frac{\delta E^{H}[\rho_{spin}]}{\delta \rho_{spin}}\right\}\left|\psi^{\beta}_i\right\rangle \qquad \forall\ \beta \text{ spin} \tag{9}$$

hence acting differently on all the α and β spin states as a consequence of the definition of ρ_{spin}. It must be remarked, in passing, that this approach works fine for systems not affected by large spin contamination. A monitoring of the SIC contribution to the various electronic states has shown that indeed the major effect is on the last singly occupied electronic level with almost negligible effects on the highest doubly occupied valence state. The fact that the energy level of $(e^-)_{aq}$ is rather far from the valence orbital (Figure 8) makes the effects of the SIC very weak on those states. This was, instead, more evident in a DNA radical on which we did this identical analysis[56,57] and where the last singly occupied energy level was a valence band state and not a well separated, and weakly interacting, gap state. The parametrized SIC of eq 1 and 9 requires a careful testing of the prefactor a_{SIC} that was found to have an optimal value of 0.2 in ref 33. In this specific case, the parameter a_{SIC} was varied in the range [0.2, 0.7] and the optical spectrum was computed according to the formula

$$\sigma(\omega) = \text{const}\,\frac{1}{\hbar\omega}\sum_{i,j}(f_i - f_j)|\langle\psi_i|\mathbf{p}|\psi_j\rangle|^2\delta(\epsilon_i - \epsilon_j - \hbar\omega) \tag{10}$$

where ψ_i and ϵ_i are the eigenstates and eigenvalues of the KS Hamiltonian, f_i is the corresponding occupation number ($f_i = 0, 1$), and $\mathbf{p}$ the momentum operator; the difference $(f_i - f_j)$ ensures a fermionic occupancy. The results, in terms of the position of the peak corresponding to the maximum of $\sigma(\omega)$, are summarized in Table 1. Measurements relevant to the HDSW system considered here were never reported, thus the closest available data[25] at $T = 618$ K and $\rho = 0.65$ g/cm^3 have been included in the table, although relative to near-critical and not supercritical water.

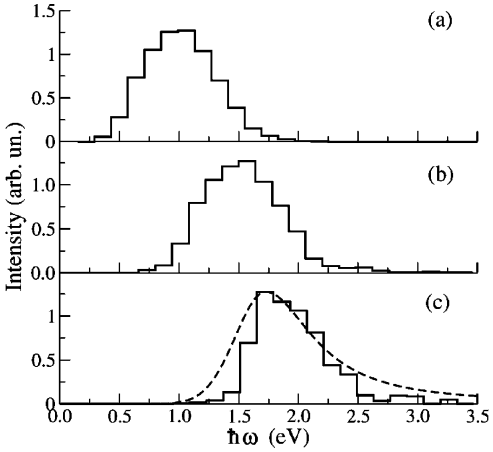

Figure 9. Optical absorption spectra for the three thermodynamic states of water considered here: (a) LDSW; (b) HDSW; (c) NLW. The solid histograms refer to the present calculations with a scaling parameter $a_{SIC} = 0.3$ for the self-interaction correction to the Hartree functional, and the dashed line is the experimental curve of ref 3.

It must be acknowledged that if SIC effects are not included, the quality of the results is already rather good. As pointed out in ref 14, this good agreement is somehow fortuitous because of the almost correct energy separation between the hydrated electron level and the empty p-like states. However, it must be stressed that, in general, transitions $\epsilon_i \rightarrow \epsilon_j$ are generally affected by a red shift if valence-conduction states are involved due to the gap underestimation affecting present-day DFT approaches.

By looking at Table 1, it turns out that the inclusion of SIC, despite being a minor correction, improves in a systematic way the agreement with the experiment, showing that unpaired electrons are always more or less affected by self-interaction problems in DFT approaches. In this specific case, the best agreement with available experimental data and former path integral simulations is given by $a_{SIC} = 0.3$, a value not too distant from $a_{SIC} = 0.2$ obtained in ref 33, where, as mentioned, the SIC correction was applied only to the last singly occupied level of the training set of systems adopted. Larger values of the parameter a_{SIC} lead to an overcorrection that was already pointed out in the original work of Perdew and Zunger[58] in which the Hartree spin density functional is added as in eq 1 with $a_{SIC} = 1$, i.e., without any weight factor. The improvement is mostly due to the fact that the inclusion of the SIC shifts slightly the solvated electron level toward the bulk of the empty σ^* antibonding states of the conduction band. Because the $(e^-)_{aq}$ KS level approaches the σ^* antibonding band upon decreasing the density of the fluid, as seen in the DOS (Figure 8), the effect of the SIC in terms of position of the absorption peak becomes less pronounced at low density.

The computed optical absorption spectra with $a_{SIC} = 0.3$ for the three thermodynamic states studied here are shown in Figure 9, where, in the case of NLW, the experimental curve from ref 3 is included for comparison.

The overall shape of the optical curve is barely affected by the SIC, and the only small, although systematic, improvement relies only on the position of the maximum. As expected,[15] the optical absorption spectrum reflects both the approach of the $(e^-)_{aq}$ energy level to the σ^* empty states band, in terms of position of the absolute maximum, and the degree of isotropy in the electron density distribution of $(e^-)_{aq}$, in terms of shape

of the curve. In fact, the spectrum evolves from a Lorenz-like distribution in NLW to a more symmetric Gaussian-like one in LDSW.

For the sake of completeness, as a final comment, it can be noted that the fact that the $(e^-)_{aq}$ energy level is singly occupied induces a splitting of the α and β levels. This is not unexpected as far as the singly occupied $(e^-)_{aq}$ level is concerned. The $\alpha-\beta$ splitting for this half-filled level turns out to be 0.055 (NLW), 0.069 (HDSW), and 0.118 eV (LDSW) for the three thermodynamic states studied here. In all cases the occupied α state is lower in energy with respect to its empty counterpart β by the amounts indicated above. But more interesting is the fact that also the highest doubly occupied level, i.e., the top of the valence band, although far from $(e^-)_{aq}$, undergoes a slight splitting of 0.011 (NLW), 0.005 (HDSW), and 0.002 eV (LDSW). Albeit small in these cases, the $\alpha-\beta$ splitting is systematic for any of the a_{SIC} parameters examined, including $a_{SIC} = 0$. In the systems inspected here, for the reason mentioned above, this splitting is on the verge of the numerical accuracy allowed by the computational approach adopted. Instead, a larger $\alpha-\beta$ splitting was found to affect DNA radical cations in solution,[56,57] where the singly occupied level is not a gap state but a valence state; also in that case a careful reparametrization of both a_{SIC} and b_{SIC} turned out to be necessary. From both these results, it can be argued that a spin restricted, $\alpha = \beta$, treatment for the doubly occupied states plus a spin unrestricted, $\alpha \neq \beta$, SIC on the last singly occupied state is not always a correct approach.

4. Conclusions

First principles molecular dynamics simulations of an excess electron performed at different densities and temperatures have shown how the disruption of the H-bond network is accompanied by a destabilization of the solvation shell of the hydrated electron and a reduction in the number of H_2O molecules concurring to form the hydration cage. On average, six water molecules are present in the first solvation shell of $(e^-)_{aq}$ at ordinary liquid conditions and four or less in the supercritical states where the density is lower than 1.0 g/cm^3. Yet, a non-negligible degree of localization of the excess electron is still present also at very low densities (0.32 g/cm^3), thus providing support to pioneering experiments in near critical water. A simple algorithm useful to analyze the H-bond network topology and to identify the configurations in which the solvated electron is localized has been presented along with its performance in the description of regular hydrogen bond structures in water. This computational tool has been used to select the configurations more appropriate for a deeper analysis of both the electronic structure and the solvation properties of $(e^-)_{aq}$. An inspection of the electronic density of states has shown that, in general, the hydrated electron is represented by a peak in the energy gap, more or less shifted toward the conduction band, outlining a general trend that points at larger shifts at lower densities. Finally, an inspection of the influence of the SIC on the optical spectrum has shown that self-interaction effects are indeed present in unpaired electrons in DFT, although in the present cases they seem to be marginal. Yet, the SIC represents a systematic improvement in terms of peak position of the absorption curve, mainly due to effects on the last unpaired electron state and its relative energetic location inside the gap.

Acknowledgment. I gratefully acknowledge insightful discussions with Michele Parrinello, Giacinto Scoles, Pier Luigi Silvestrelli, Michiel Sprik, and Alberto Ubaldini. I am strongly indebted to Roger Rousseau for reading the original version of this manuscript and making several crucial remarks. Calculations were performed on the computer facilities of the Science Information Processing Center, University of Tsukuba, and partly on the PACS-CS system at CCS. This work was partly supported by JST-CREST and a grant-in-aid from MEXT under contract number 18054004.

References and Notes

(1) Hart, E. J.; Boag, J. W. *J. Am. Chem. Soc*. **1962**, *84*, 4090−4095.
(2) Hart, E. J.; Anbar, M. *The Hydrated Electron*; Wiley: New York, 1970.
(3) Jou, F. Y.; Freeman, G. R. *J. Phys. Chem.* **1979**, *83*, 2383−2387.
(4) Baron, B.; Hoover, D.; Williams, F. *J. Chem. Phys*. **1978**, *68*, 1997−1999.
(5) Grand, D.; Bernas, A.; Amouyal, E. *Chem. Phys*. **1979**, *44*, 73−79.
(6) Han, P.; Bartles, D. M. *Phys. Rev. Lett*. **1990**, *64*, 1469−1472.
(7) Bragg, A. E.; Verlet, J. R. R.; Kammerath, A.; Cheshnovsky, O.; Neumark, D. M. *Science* **2004**, *306*, 669−671.
(8) Lian, R.; Crowell, R. A.; Shkrob, I. A. *J. Phys. Chem. A* **2005**, *109*, 1510−1520.
(9) Schnikter, J.; Rossky, P. J. *J. Chem. Phys.* **1987**, *86*, 3471−3485.
(10) Schnikter, J.; Motakabbir, K.; Rossky, P. J.; Friesener, R. A. *Phys. Rev. Lett*. **1988**, *60*, 456−459.
(11) Webster, F. J.; Schnikter, J.; Friedrichs, M. S.; Friesener, R. A.; Rossky, P. J. *Phys. Rev. Lett.* **1991**, *66*, 3172−3175.
(12) Barnett, R. N.; Landman, U.; Cleveland, C. L.; Jortner, J. *J. Chem. Phys*. **1988**, *88*, 4421−4428.
(13) Kim, K. S.; Park, I. J.; Lee, S.; Cho, K.; Lee, J. M.; Kim, J.; Joannoupulos, J. D. *Phys. Rev. Lett*. **1996**, *76*, 956−959.
(14) Sprik, M.; Impey, R. W.; Klein, M. L. *J. Stat. Phys.* **1986**, *43*, 967−972.
(15) Boero, M.; Parrinello, M.; Terakura, K.; Ikeshoji, T.; Liew, C. C. *Phys. Rev. Lett*. **2003**, *90*, 226403.
(16) Ludwig, V.; Coutinho, K.; Canuto, S. *Phys. Rev. B* **2004**, *70*, 214110.
(17) Tavernelli, I. *Phys. Rev. B* **2006**, *73*, 094204.
(18) Shkrob, I. A.; Sauer, M. C. *J. Phys. Chem. A* **2005**, *109*, 5754−5769.
(19) Neumark, D. M. *J. Chem. Phys*. **2006**, *125*, 132303.
(20) Smallwood, C. J.; Bosma, W. B.; Larsen, R. E.; Schwartz, B. J. *J. Chem. Phys*. **2003**, *119*, 11263−11277.
(21) Bernasconi, L.; Sprik, M.; Hutter, J. *J. Chem. Phys.* **2003**, *119*, 12417−12431.
(22) Blumberger, J.; Bernasconi, L.; Tavernelli, I.; Vuilleumier, R.; Sprik, M. *J. Am. Chem. Soc*. **2004**, *126*, 3928−3938.
(23) Herbert, J. M.; Head-Gordon, M. *J. Am. Chem. Soc*. **2006**, *128*, 13932−13939.
(24) Bedard-Hearn, M. J.; Larsen, R. E.; Schwartz, B. J. *J. Chem. Phys.* **2006**, *125*, 194509.
(25) Gaathon, A.; Czapski, G.; Jortner, J. *J. Chem. Phys.* **1973**, *58*, 2648−2650.
(26) Gallot, G.; Bratos, S.; Pommeret, S.; Lascoux, N.; Leicknam, J. C.; Kozinski, M.; Amir, W.; Gale, G. M. *J. Chem. Phys.* **2002**, *117*, 11301−11309.
(27) Laria, D.; Skaf, M. S. *J. Phys. Chem. A* **2002**, *106*, 8066−8069.
(28) Ikushima, Y.; Hatakeda, K.; Sato, O.; Yokoyama, T.; Arai, M. *Angew. Chem., Int. Ed.* **1999**, *38*, 2910−2194.
(29) Bröll, D.; Kaul, C.; Krämer, A.; Krammer, P.; Richter, T.; Jung, M.; Vogel, H.; Zehner, P. *Angew. Chem., Int. Ed.* **1999**, *38*, 2999−3014.
(30) Marin, T. W.; Cline, J. A.; Takahashi, K.; Bartles, D. M.; Jonah, C. D. *J. Phys. Chem. A* **2002**, *106*, 12270−12279.
(31) Boero, M.; Ikeshoji, T.; Liew, C. C.; Tearkura, K.; Parrinello, M. *J. Am. Chem. Soc*. **2004**, *126*, 6280−6286.
(32) Laegsgaard, J.; Stokbro, K. *Phys. Rev. Lett*. **2001**, *86*, 2834−2837.
(33) VandeVondele, J.; Sprik, M. *Phys. Chem. Chem. Phys*. **2005**, *7*, 1363.
(34) Car, R.; Parrinello, M. *Phys. Rev. Lett.* **1985**, *55*, 2471−2474.
(35) CPMD; Copyright IBM Corp. 1990−2001; Copyright MPI für Festkörperforschung, Stuttgart, 1997−2004.
(36) It has been proven in refs 37 and 38 that the use of either a 32- or a 64-molecule model system leads to numerically identical results.
(37) Silvestrelli, P. L.; Parrinello, M. *Phys. Rev. Lett.* **1999**, *82*, 3308−3311.
(38) Silvestrelli, P. L.; Parrinello, M. *J. Chem. Phys.* **1999**, *111*, 3572−3580.
(39) Boero, M.; Terakura, K.; Ikeshoji, T.; Liew, C. C.; Parrinello, M. *Phys. Rev. Lett.* **2000**, *85*, 3245−3248.
(40) Boero, M.; Terakura, K.; Ikeshoji, T.; Liew, C. C.; Parrinello, M. *J. Chem. Phys.* **2001**, *115*, 2219−2227.

(41) Nosé, S. *Mol. Phys*. **1984**, *52*, 255−268.
(42) Nosé, S. *J. Chem. Phys*. **1984**, *81*, 511−519.
(43) Hoover, W. G. *Phys. Rev. A* **1985**, *31*, 1695−1697.
(44) Becke, A. D. *Phys. Rev. A* **1988**, *38*, 3098−3100.
(45) Lee, C.; Yang, W.; Parr, R. G. *Phys. Rev. B* **1988**, *37*, 785−789.
(46) Troullier, N.; Martins, J. L. *Phys. Rev. B* **1991**, *43*, 1993−2006.
(47) Sprik, M.; Hutter, J.; Parrinello, M. *J. Chem. Phys.* **1996**, *105*, 1142−1152.
(48) Schwegeler, E.; Grossman, J. C.; Gygi, F.; Galli, G. *J. Chem. Phys.* **2005**, *121*, 5400−5409.
(49) Marzari, N.; Vanderbilt, D. *Phys. Rev. B* **1997**, *56*, 12847−12865.
(50) Resta, R.; Sorella, S. *Phys. Rev. Lett*. **1999**, *82*, 370−373.
(51) Gregory, J. K.; Clary, D. C.; Liu, K.; Brown, M. G.; Saykally, R. J. *Science* **1997**, *275*, 814−817.
(52) Keutsch, F. N.; Saykally, R. J. *Proc. Natl. Acad. Sci. U.S.A.* **2001**, *98*, 10533−10540.
(53) Boero, M.; Ikeshoji, T.; Terakura, K. *ChemPhysChem* **2005**, *6*, 1775−1779.
(54) Pendergast, D.; Grossman, J. C.; Galli, G. *J. Chem. Phys.* **2005**, *123*, 014501.
(55) d'Avezac, M.; Calandra, M.; Mauri, F. *Phys. Rev. B* **2005**, *71*, 205210.
(56) Gervasio, F. L.; Boero, M.; Parrinello, M. *Angew. Chem. Int. Ed*. **2006**, *45*, 5606−5609.
(57) Boero, M.; Gervasio, F. L.; Parrinello, M. *Mol. Simul.* **2007**, *33*, 57−60.
(58) Perdew, J. P.; Zunger, A. *Phys. Rev. B* **1981**, *23*, 5048−5079.